Engineering 28 (2023) 153–165

Contents lists available at ScienceDirect

Engineering

journal homepage: www.elsevier.com/locate/eng

Research
Green Plant Protection Innovation—Article

Pseudomonas Cyclic Lipopeptide Medpeptin: Biosynthesis and Modulation of Plant Immunity

Yi-Lin Gu [a,#], Jun-Zhou Li [a,#], Yan Li [b], Shen Cong [a], Jing Wang [a], Yi-Nan Ma [a], Hai-Lei Wei [a,*]

[a] State Key Laboratory of Efficient Utilization of Arid and Semi-arid Arable Land in Northern China, Key Laboratory of Microbial Resources Collection and Preservation, Ministry of Agriculture and Rural Affairs, Institute of Agricultural Resources and Regional Planning, Chinese Academy of Agricultural Sciences, Beijing 100081, China
[b] Institute of Vegetables and Flowers, Chinese Academy of Agricultural Sciences, Beijing 100081, China

ARTICLE INFO

Article history:
Received 20 January 2023
Revised 16 March 2023
Accepted 18 May 2023
Available online 23 July 2023

Keywords:
Pseudomonas
Cyclic lipopeptide
Cell death
Leucine-rich repeat extension (LRX)
Medpeptin
Receptor-like kinase (RLK)

ABSTRACT

The multifunctional secondary metabolites known as cyclic lipopeptides (CLPs), which are produced by a large variety of bacteria, have become a key category of plant immunity elicitors. *Pseudomonas*-CLPs (Ps-CLPs) are extremely diverse in structure and biological activity. However, an understanding of CLP-plant structure–function interactions currently remains elusive. Here, we identify medpeptin, a novel CLP from *Pseudomonas mediterranea* that consists of 22 amino acids. Medpeptin is synthesized by a non-ribosomal peptide synthase (NRPS) gene cluster and regulated by a quorum-sensing system. Further research indicates that medpeptin does not exhibit antimicrobial activity; instead, it induces plant cell death immunity and confers resistance to bacterial infection. Comparative transcriptome analysis and virus-induced gene silencing (VIGS) reveal a set of immune signaling candidates involved in medpeptin perception. Silencing of a cell-wall leucine-rich repeat extensin protein (NbLRX3) or a receptor-like protein kinase (NbRLK25)—but not BAK1 or SGT1—compromises medpeptin-triggered cell death and resistance to pathogen infection in *Nicotiana benthamiana*. Our findings point to a noncanonical mechanism of CLP sensing and suggest perspectives for the development of plant disease resistance.

1. Introduction

Soil-dwelling and plant-associated *Pseudomonas* species are known for their biological activity of controlling plant diseases, either directly by producing antagonistic metabolites or indirectly by inducing plant defense resistance responses [1,2]. Cyclic lipopeptides (CLPs) are a large class of secondary metabolites produced by a wide range of *Pseudomonas* strains; they have attracted significant interest because of their antimicrobial, cytotoxic, and plant resistance-inducing properties [3,4]. The massive increase in *Pseudomonas* whole-genome sequences has led to the discovery of more diverse CLP products. Revealing the CLP spectrum and determining the multiple activities of these secondary metabolites could establish a framework for developing and selecting effective biological controls and plant resistance strategies.

CLPs comprise a cyclic oligopeptide lactone ring linked with a fatty acid tail. Most CLPs are synthesized by a large non-ribosomal peptide synthase (NRPS) cluster, which is composed of multi-domain modules, with each module catalyzing the modification and addition of amino acids [4,5]. Every module consists of three core domains: aminoacyl-adenylation (A), thiolation (T), and condensation (C) domains [6]. To date, 100 or more *Pseudomonas*-CLPs (Ps-CLPs) have been identified and divided into at least 14 groups based on the composition and length of the fatty acid tail, as well as the kind, amount, and configuration of the amino acids in the peptide moiety [5]. The *P. fluorescens* complex co-synthesizes two kinds of Ps-CLPs from the mycin and peptin families. Members of the mycin family have a fully cyclized peptide with nine amino acids, while peptin family members are larger CLPs composed of a partially cyclized peptide ranging in length from 19 to 25 amino acids [7]. CLP biosynthetic gene clusters (BGCs) are typically spread across a large genomic island of more than 100 kb. Transporter-encoding genes of CLPs are located downstream of the last synthetase gene, whereas regulatory genes such as *luxR* homologs are positioned upstream or downstream of CLP structure genes [8,9]. It has been shown that *P. corrugata* encodes an *N*-acyl-homoserine lactone quorum sensing (AHL-QS) system, PcoI/PcoR, which regulates downstream LuxR expression

* Corresponding author.
E-mail address: weihailei@caas.cn (H.-L. Wei).
# These authors contributed equally to this work.

https://doi.org/10.1016/j.eng.2023.05.016

and controls the production of CLPs and antimicrobial activity [10–12]. Additional examples of the LuxR-type regulation of CLPs have been reported in soil-dwelling and plant-associated *Pseudomonas* species [8,13].

Interest in CLPs has been driven primarily by their antimicrobial and surfactant activities; however, awareness of their functions is being considerably broadened, most notably with the recent remarkable discovery that they comprise a key category of plant immunity elicitors. Along with other microbe-derived plant immunity elicitors, CLPs are known as invasion patterns (IPs) [14]. Plants deploy cell-surface pattern-recognition receptors (PRRs) to perceive extracellular IPs, such as flg22 or elf18, and initiate pattern-triggered immunity (PTI) responses, such as reactive oxygen species (ROS) burst, callose deposition, mitogen-activated protein kinase (MAPK) cascades, and large-scale transcriptional programming [15]. In contrast, intracellular nucleotide-binding leucine-rich repeat proteins (NLRs) can recognize intracellular effectors, resulting in a hypersensitive response (HR) or local cell death, which restricts pathogen proliferation [15]. Several studies have reported that CLPs are involved in stimulating plant resistance in various pathosystems. Massetolide A from *P. fluorescens* SS101 was shown to induce local and systemic resistance in tomatoes against *Phytophthora infestans* (*P. infestans*) [16]. *P. protegens* and related species can synthesize orfamide-type CLPs, which not only have insecticidal activity [17] but also trigger plant immune responses against *Cochliobolus miyabeanus* or *Rhizoctonia solani* in rice, bean, and cabbage [18–20]. Corpeptin and cormycin are two major CLPs synthesized in *P. corrugata*, both of which have antimicrobial activity, the ability to induce cell death, K^+/H^+ exchange, and an active oxygen burst in tobacco [21,22]. In contrast to other IPs, there has been no indication so far of the involvement of specific PRRs or NLRs in the perception of CLPs directly. However, it is noteworthy that an increasing number of studies have emphasized the significance of PRRs in the recognition of bacterial IPs containing fatty acids and/or oligopeptides. A surface-localized lectin S-domain receptor kinase (LORE/SD1-29) has been reported to sense the bacterial outer cell membrane component lipopolysaccharide (LPS) and mount innate immune responses [23]. Moreover, synthetic and bacterial LPS-copurified medium-chain 3-hydroxy fatty acid (mc-3-OH-FA) metabolites elicit LORE-dependent immunity in *Arabidopsis* [24]. Recently, Schellenberger et al. [25] revealed that the 3-hydroxyalkanoate precursors of bacterial rhamnolipids are sensed by LORE to activate *Arabidopsis* innate immunity, whereas rhamnolipids induce RBOHD-dependent long-lasting oxidative bursts. In addition, cell-wall-associated proteins, such as leucine-rich repeat extensions (LRXs), have been shown to be involved in peptide recognition and immune regulation [26]. As a result, we question whether CLPs can be sensed by cell-surface proteinaceous receptors to modulate plant immunity.

P. mediterranea S58 is a plant growth-promoting rhizobacterium that antagonizes a series of plant pathogenic fungi and bacteria and induces cell death immunity in *Nicotiana benthamiana* (*N. benthamiana*) [27]. Genome analysis has demonstrated that *P. mediterranea* S58 has no type-III secretion system (T3SS) but produces multiple CLPs synthesized by large non-ribosomal peptide synthetase (NPRS) gene clusters. In this article, we report that the NPRS gene cluster (BGC7) determines cell death immunity but not antimicrobial activity. Using high-performance liquid chromatography (HPLC) and tandem mass spectrometry (MS/MS), we identified a novel CLP, which we denote as medpeptin, with 22 amino acids, synthesized by BGC7 and regulated by a flanked quorum-sensing (QS) system. We performed a comparative transcriptomic analysis to identify a set of signaling genes that respond to medpeptin perception in *N. benthamiana*. Virus-induced gene silencing (VIGS) revealed that a cell-wall leucine-rich repeat extensin and a receptor-like protein kinase are critical for the cell death immunity triggered by medpeptin and *P. mediterranea* S58. Our study, therefore, reveals a noncanonical mechanism of CLP-plant interactions. These new insights into the CLP modulation of plant immunity pave the way for a promising biotechnological application for plant disease protection.

2. Materials and methods

2.1. Bacterial strains and plasmids

The bacterial strains and plasmids utilized in this study are listed in Table S1 in Appendix A. King's B (KB) medium was used to cultivate *P. mediterranea* S58 and derivatives at 28 °C [28], while *Escherichia coli* (*E. coli*) strains and *Agrobacterium tumefaciens* (*A. tumefaciens*) GV3101 were grown at 37 and 28 °C, respectively, in Luria-Bertani (LB) medium containing appropriate antibiotics.

2.2. Construction of a P. mediterranea S58 transposon mutant library

Transposon mutagenesis of *P. mediterranea* S58 was carried out by means of biparental mating with recipient cell S58 and donor cell *E. coli* S17-1 λ pir carrying plasmid pUTKm [29], as described previously [30,31].

2.3. Sequence analysis and construction of P. mediterranea S58 mutants

The BGCs of the *P. mediterranea* S58 genome were predicted *in silico* using the online PRISM toolkit [32]. To mutate the BGCs, 0.8–1.2 kb flanking sequences were amplified from the upstream and downstream of each BGC using designed primers (Table S2 in Appendix A). Two flanking regions were fused and cloned into the pK303sacB plasmid; then, the completed vector was transformed into strain S58 by triparental mating with the helper plasmid pRK2013. The BGC deletions were constructed using homologous recombination and confirmed by sequencing. The *fliC* and *pcoI* mutants were created using the same method. All the primers used are listed in Table S2. To perform phylogenetic analysis of *MIG25* and *MIG28* genes, homologs from different plant species were searched through the Basic Local Alignment Search Tool (BLAST) and downloaded from the National Center for Biotechnology Information (NCBI) database. Phylogenetic trees of MIG25 and MIG28 were constructed using the neighbor-joining algorithm in the MEGA software (v 7.0) with a bootstrap analysis of 1000 replications.

2.4. ROS, callose deposition, and electrolyte leakage measurements

N. benthamiana plants were grown at 24 °C during the day and 22 °C at night, with a 16 h light per 8 h dark cycle. Six-week-old plants were used in all experiments. ROS bursts were detected as previously described [33,34]. Callose deposition assays were performed as previously described [35]. At 15 hour post infection (hpi) of strain S58 and its derivatives, the treated leaves were stained with aniline blue and visualized using confocal laser scanning microscopy (LSM 880; Carl Zeiss, Germany). Callose deposition was counted using the ImageJ software (v. 1.8.0). For electrolyte leakage assay, *N. benthamiana* leaves were infiltrated with 1×10^8 colony forming units (CFUs)·mL^{-1} of strain S58 and derivatives and 10 mmol·L^{-1} $MgCl_2$ (mock). The conductivity was measured using a conductivity meter (S230; Seven Compact, China) [36]. All experiments were repeated at least three times with multiple replicates.

2.5. RNA sequencing and quantitative reverse transcription polymerase chain reaction (qRT-PCR) assay

N. benthamiana leaves were inoculated with a bacterial suspension at 1×10^8 CFU·mL^{-1} or extract at 100 nmol·L^{-1}. The leaf discs were taken at 6 hpi for total RNA preparation. Libraries were constructed and sequenced using an Illumina HiSeq platform (GENEWIZ Ltd., China). The reads were trimmed and aligned to the *N. benthamiana* genome sequence [37]. Differentially expressed genes (DEGs) were identified using DESeq2 (v. 1.6.3) [38]. A false discovery rate (FDR) ≤ 0.05 and fold change ≥ 2 were set as cutoffs for significant DEGs. The R package pheatmap (v. 1.0.12), with Pearson's correlation and average linkage clustering, was used to create heatmaps. Venn diagrams were used to screen for overlapping genes among treatments [39]. Gene ontology (GO) terms and enrichment analysis of candidate DEGs were performed using the R package topGO (v. 2.48.0), with a cutoff at $P < 0.05$. The candidate DEGs involved in biotic stress responses and metabolic pathways in plants were predicted and visualized using MapMan software (3.5.1) [40]. Protein–protein interaction (PPI) network analysis was performed using *Arabidopsis* homologs, because PPI data and analysis resources were readily available. PPI analysis of the *Arabidopsis* homologs predicted from the *N. benthamiana* network string-interacting proteins was carried out using the STRING database [41].

The expression of candidate DEGs was verified using qRT-PCR which was performed as previously described [27]. The $2^{-\Delta\Delta Ct}$ method was used to calculate the expression levels, which were standardized to the level of constitutively expressed *NbEF1α* and normalized to expression in mock cells. All experiments were repeated at least three times.

2.6. Virus-induced gene silencing in N. benthamiana

The target regions for gene silencing were designed using the SGN VIGS Tool [42] and were amplified from the complementary DNA (cDNA) of *N. benthamiana* using appropriate primers (Table S2). The resulting PCR products were integrated into pCR8/GW/TOPO (Life Technologies, USA) and recombined into the TRV2 destination vector via the Gateway cloning technique [43,44] with LR clonase II (Life Technologies). The constructs were sequenced for confirmation and transformed into *A. tumefaciens* GV3101 by means of electroporation. VIGS was performed as previously described [45,46]. *A. tumefaciens* GV3101 harboring pTRV1, pTRV2-*EC1*, pTRV2-*PDS*, and pTRV-target genes from *N. benthamiana* was cultured on LB plates supplemented with appropriate antibiotics. All experiments were repeated at least three times, with multiple replicates.

2.7. Extraction and purification of the lipopeptide

Strain S58 was inoculated into 5 mL of LB broth at 28 °C and 200 rpm for 12 h, then diluted 1:1000 into 1 L flasks containing 300 mL of LB broth and cultured for 48 h under the same conditions. The organic fractions of the fermentation were separated after three separate extractions with an ethyl acetate solution of an equal volume, and the organic fractions were collected and evaporated under vacuum to yield the crude extracts. The extract was purified using preparative reverse-phase high-performance liquid chromatography (prep-HPLC) using a Hanbon DAC 100 (Hanbon, China) equipped with a DAC C18 column (50 mm × 250 mm, filler diameter: 10 μm), and liquid chromatography-tandem mass spectrometry (LC-MS/MS) was used to analyze the products. The fractions were then separated in two steps. First, the extract was collected through a gradient elution from 80% acetonitrile containing 0.1% trifluoroacetic acid and 20% water containing 0.1% formic acid to 100% acetonitrile containing 0.1% trifluoroacetic acid over 40 min; it was then kept in 100% acetonitrile containing 0.1% trifluoroacetic acid for 200 min at a flow rate of 80 mL·min^{-1} and 210 nm. Eluates were collected at 0–15, 16–30, and 60–75 min and analyzed using matrix-assisted laser desorption/ionization time-of-flight mass spectrometry (MALDI-TOF MS) with an Autoflex II Spectrometer (Bruker, Germany) for lipopeptide detection. Second, the eluate containing the target lipopeptide was purified using the above equipment, and the elution conditions were modified. A gradient elution was performed from 65% acetonitrile including 0.1% trifluoroacetic acid and 35% water including 0.1% formic acid to 80% acetonitrile including 0.1% trifluoroacetic acid over 40 min; then, the acetonitrile including 0.1% trifluoroacetic acid was increased to 85% from 40 to 50 min and maintained at 85% acetonitrile including 0.1% trifluoroacetic acid for 110 min under the same conditions. The eluate from the single peak was collected, lyophilized, and stored at −80 °C.

2.8. Determination of the molecular structure of medpeptin

The target peptides in the cells, crude extracts, and fractions were identified by means of MALDI-TOF MS using prep-HPLC. Fresh cells were suspended in saturated substrate solution with a 1:1 mixture of 2,5-dihydroxybenzoic acid (DHBA) and a-cyano-4-hydroxycinnamic acid (HCCA), and the extract was dissolved in a 1:1 solution of methanol and the substrate. The sample was then spotted and dried on an anchor plate. Data were acquired in the positive reflection mode, ranging from 500 to 2500 Da. FlexAnalysis 3.4 software (Bruker Autoflex MALDI-TOF; Bruker was used to analyze single-spot MALDI-TOF MS data.

To further identify the molecular structure of medpeptin, the A, T, C, and thioesterase (TE) domains of NRPS genes were identified using PFAM[†]. LC-MS/MS was performed using an ABScieX TripleTOF 6600 mass spectrometer (AB SCIEX, USA) in positive ion mode equipped with a nano-electrospray source. The electrospray parameters were as follows: ionspray voltage, 5.5 kV; heated inlet temperature, 550 °C; nebulizing gas pressure, 25 pounds per square inch (psi); N_2 collision-induced dissociation energy, 145 V; and peak resolution, 40 k.

2.9. Statistical analysis

The NCBI database's accession number for the raw is PRJNA861400. Statistical significance was calculated using Tukey's honestly significant difference (HSD) test with SPSS software (v. 22.0) and defined with P values less than 0.05. The experiments were repeated more than three times, and representative results are presented as mean ± standard deviation (SD).

3. Results

3.1. Identification of P. mediterranea genes involved in cell death induction

We previously discovered that *P. mediterranea* S58 could induce cell death immunity in *N. benthamiana* [27]. However, no T3SS homologs were found in the S58 genome, ruling out T3SS-dependent cell death. We then deployed forward genetics to generate a Tn5 transposon insertion library with 14 976 colonies to screen for mutants deficient in cell death elicitation. Antimicrobial mutants were screened to determine the functional dichotomy of the strain S58. Twelve mutants showed deficient cell death or

[†] http://www.sanger.ac.uk/Software/Pfam/.

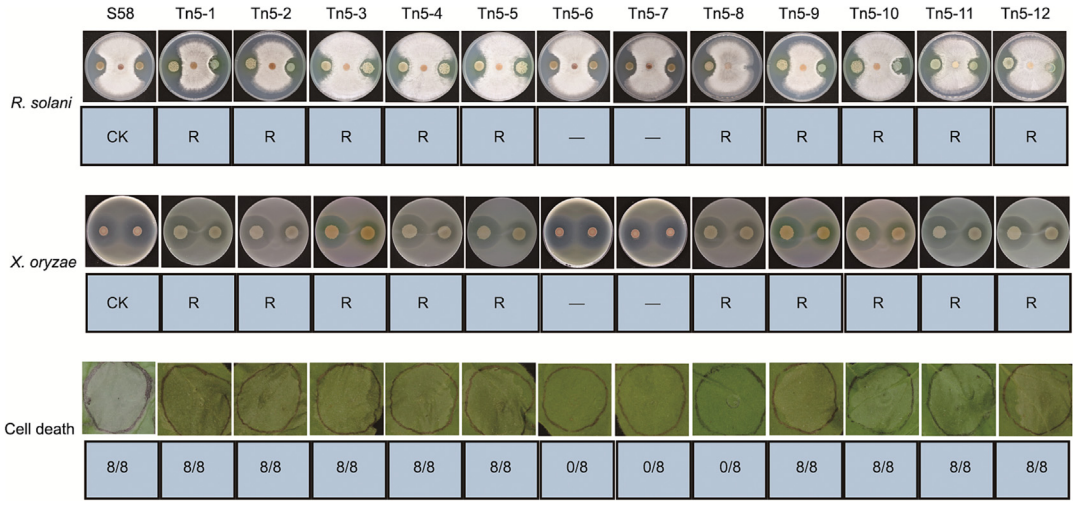

Fig. 1. Screening of antagonism- and cell death-deficient mutants. *R. solani* and *Xanthomonas oryzae* were used as a plant pathogenic fungus and bacterium, respectively, to screen *P. mediterranea* mutants. Fungal discs were placed on the potato dextrose agar (PDA) plate center, and the bacterial suspension was mixed with LB media. Strain S58 and single mutants were placed on the left and right side of each plate, respectively. Antimicrobial activity was measured by the diameter (mm) of the clear zone of growth inhibition. Strain S58, on the right side of the first plate, was used as a control (CK). "R" represents reduced antimicrobial activity of a mutant compared with wild-type strains S58. "—" represents no difference. Cell-death-deficient mutants of *P. mediterranea* S58 were screened in *N. benthamiana*. Bacterial suspensions at 5×10^8 CFUs·mL^{-1} were infiltrated into the marked zones of plant leaves, and the leaf response was photographed two days later. The fraction under each image indicates the number of times tissue death was observed relative to the number of test inoculations. All experiments were repeated three times, with similar results.

antimicrobial activity (Fig. 1). Among these, ten mutants showed significantly reduced antagonistic activity against *R. solani* and *Xanthomonas oryae*, whereas only three mutants failed to cause cell death in *N. benthamiana* (Fig. 1). Interestingly, only Tn5-8 exhibited deficiencies in both antagonistic activity and induction of cell death. Tn5-6 and Tn5-7 lost the ability to induce cell death but maintained their full antimicrobial activity, whereas the rest had the opposite effect (Fig. 1). We unveiled the insertion sites of all mutants that are associated with the five genes that encode aspartate-tRNA ligase, aspartate aminotransferase family protein, NRPS, acyl-homoserine lactone synthase, and glutamine synthetase (Table S3 in Appendix A). Notably, some mutants were inserted by Tn5 at different sites within the same gene, such as Tn5-6 and Tn5-7—two cell-death-deficient mutants that had mutations in the NRPS gene (Table S3).

As a complementary strategy, we used genome mining and site-specific mutations to identify gene clusters involved in antagonism and cell death. Nine BGCs were predicted from *P. mediterranea* S58 using PRISM, as shown in Fig. 2(a) and Table S4 in Appendix A. Using genome *in silico* prediction, we found that BGC6, BGC7, and BGC8 were sequentially connected as gene islands (Fig. S1(a) in Appendix A). Overall, the large gene island was homologous to those found in *P. mediterranea* CFBP 5447, *Pseudomonas* sp. SH-C52, *P. corrugata* DSM 7228, and *P. fluorescens* In5 (Fig. S1(a)) [11,47–49]. Among these, BGC6 comprises nine genes, including a *pcoI/pcoR* QS system and a *pcoABC* operon (Fig. 2(a) and Table S4). BGC7 contains three NRPS genes whose homologs synthesize CLPs, such as thanapeptin, corpeptin, and nunapeptin in the corresponding *Pseudomonas* strains, whereas the BGC8 homologs synthesize thanamycin, cormycin, and nunamycin (Fig. S1(a)) [21,48,49]. In line with previous terminology, we named the potential CLP products of BGC7 and BGC8 in *P. mediterranea* S58 "medpeptin" and "medmycin" , respectively. The NRPS genes for medpeptin and medmycin were correspondingly designated as *mepABC* and *medAB*, respectively (Fig. 2(a); Fig. S1(b) in Appendix A). Compared with the insertion sites of the Tn5 mutants, BGC6 covers the *pcoI* gene disrupted in Tn5-8, whereas BGC7 covers the *mepC* gene inserted in Tn5-6 and Tn5-7 (Fig. 2(a)). With the exception of BGC4 and BGC9, we made unmarked deletions in the other seven BGCs and tested their antimicrobial and cell death activities. The results demonstrated that S58ΔBGC6 (deletion of *pcoABC*) and S58ΔBGC7 (deletion of *mepABC*) failed to trigger cell death in *N. benthamiana*, whereas only S58ΔBGC6 exhibited reduced antimicrobial activity (Fig. 2(a)). MALDI-TOF was then used to determine the bacterial metabolite profiles to confirm whether the BGC mutants were deficient in metabolite production. As shown in Fig. 2(b), S58ΔBGC6 and S58ΔBGC7 had missing molecules from *m/z* 2050 to *m/z* 2200 when compared with the wild-type strain S58. Given that BGC7 is responsible for medpeptin production, we propose that the mass of medpeptin ranges from *m/z* 2050 to *m/z* 2200.

3.2. QS positively controls the expression of BGC7 and BGC8, cell death elicitation, and antimicrobial activity of P. mediterranea

We discovered that the *pcoABC* operon (S58ΔBGC6) is associated with medpeptin production, antimicrobial activity, and cell death in *N. benthamiana*. To examine whether the QS system in BGC6 regulates the expression of BGC7 and BGC8, we constructed a *pcoI* mutant instead of using the Tn5-8 transposon mutant. The results of qRT-PCR showed that the transcriptional expression of either *mepA*, *mepB*, and *mepC* from BGC7 or *medA* and *medB* from BGC7 was blocked in the *pcoI* mutant (Fig. 3(a)). Moreover, S58Δ*pcoI* exhibited the same missing molecules from *m/z* 2050 to *m/z* 2200 as the *pcoABC* mutant, as measured by MALDI-TOF (Fig. 3(b)), indicating that the QS system positively regulates medpeptin production. We then investigated whether QS controls *P. mediterranea*-induced cell death and antimicrobial activity. As shown in Fig. 3(c), the *pcoI* mutant failed to induce cell death in *N. benthamiana* and exhibited a reduced antagonistic effect against plant pathogens, which was consistent with Tn5-8 and S58ΔBGC6 (Figs. 1 and 2(a)). We investigated whether BGC7 and BGC8 have redundancy, because single mutants of BGC7 and BGC8 showed no difference in antimicrobial activity compared with strain S58. A double mutant of BGC7 and BGC8, S58ΔBGC7ΔBGC8, showed the same antimicrobial activity as strain S58 and the single mutants (Figs. 3(c) and 2(a)). Collectively, our findings revealed that none of the known BGCs of *P. mediterranea* S58 are involved in plant pathogen antagonism; QS controls BGC7 expression, medpeptin production, plant cell death, and an undisclosed antimicro-

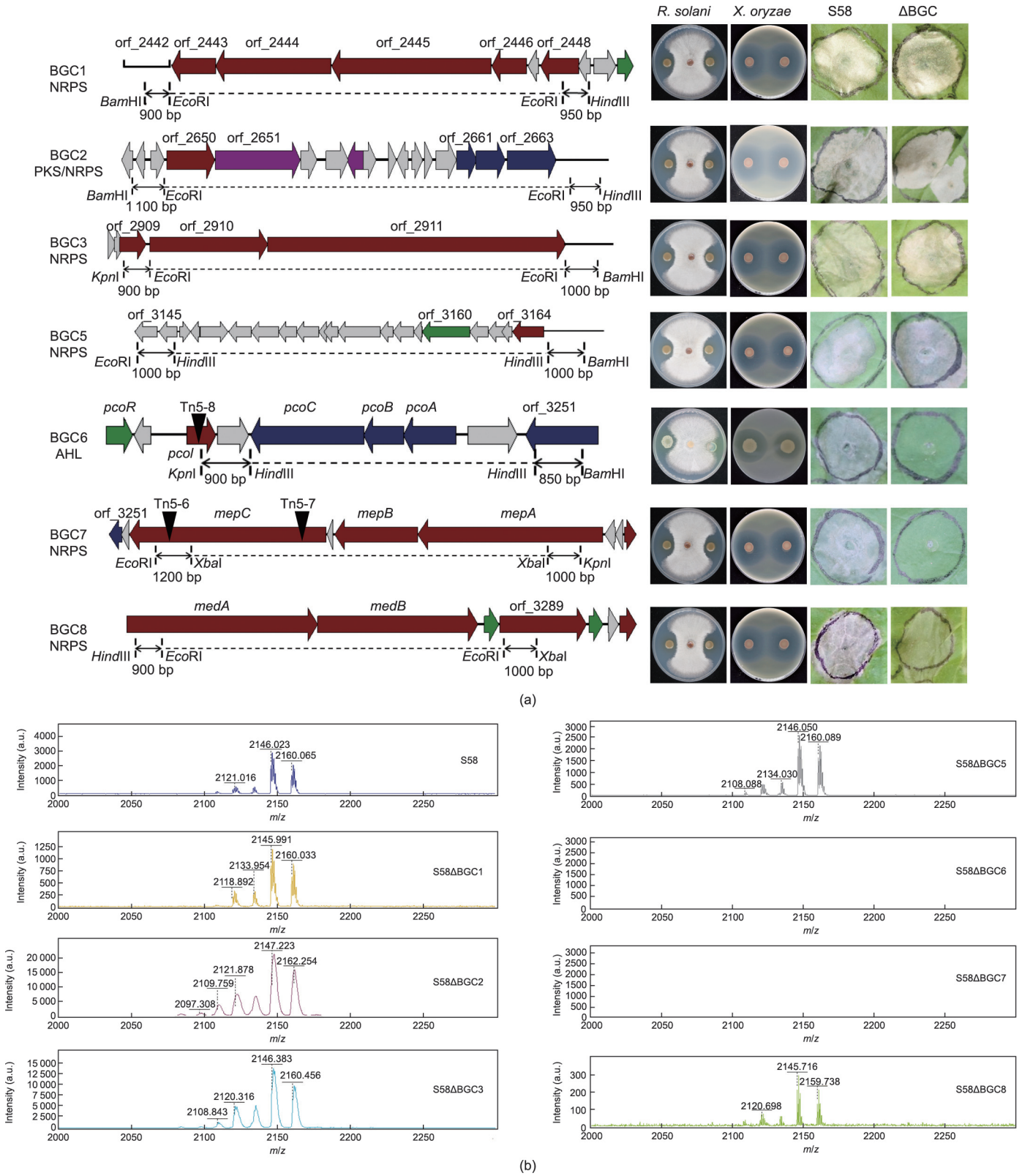

Fig. 2. Generation and characterization of the mutants of the seven BGCs. (a) *In silico* prediction of BGCs using PRISM and mutant construction via double recombination. Predicted open reading frames and their orientation are indicated by open arrows. Red, blue, green, purple, and gray arrows represent core biosynthetic genes, transport-related genes, regulatory genes, additional biosynthetic genes, and other accessory genes, respectively. Two-way arrows represent the fragments used to insert mutations. Dashes represent deleted fragments. Black triangles represent the insertion sites of the Tn5 random mutants. Antimicrobial activity and cell death were examined as shown in Fig. 1. (b) Metabolic profiles of *P. mediterranea* S58 and the deletion mutants. Extracts of the bacterial supernatants were analyzed using MALDI-TOF. The mutants of BGC6 and BGC7 failed to produce the major molecules from *m/z* 2050 to *m/z* 2200. orf: open reading frame.

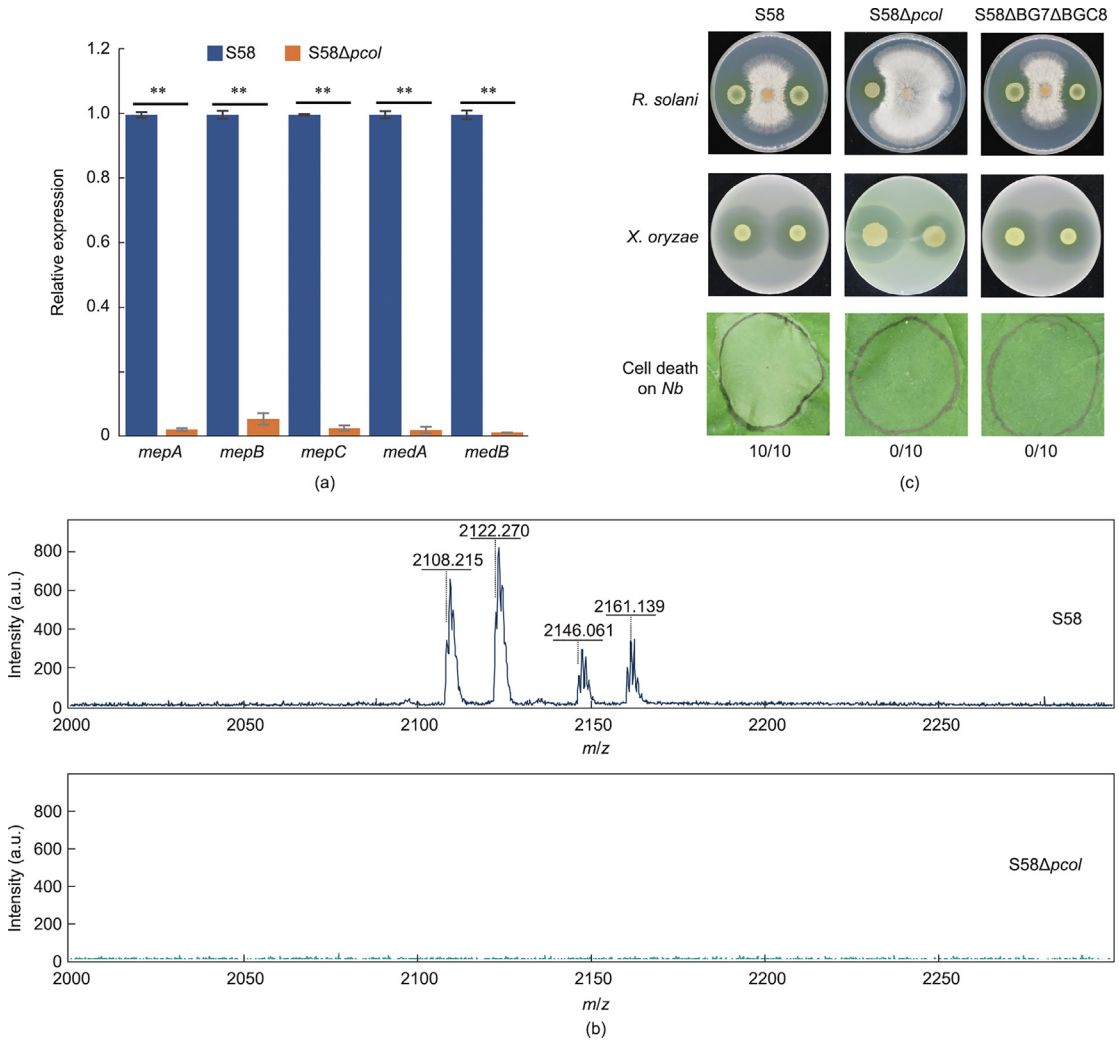

Fig. 3. QS controls the expression of BGC7 and BGC8 and biological activities. (a) Expression of *mepA*, *mepB*, and *mepC* in BGC7 and *medA* and *medB* in BGC8 was positively regulated by *pcol*. The expression levels of all genes were standardized to the level of the constitutively expressed *recA* and normalized to wild-type expression. Relative gene expression levels were calculated using the $2^{-\Delta\Delta Ct}$ method. Data shown are the means ± SD from three independent experiments; ** $P < 0.01$. (b) The *pcol* mutant is deficient in producing molecules from *m/z* 2000 to *m/z* 2300. (c) QS controls antimicrobial activity and cell death. The antagonism assay and cell death assay were performed as described in Fig. 1. All experiments were repeated three times, with similar results. *Nb: Nicotiana benthamiana.*

bial product. As we aimed to decipher the cell death inducer and its mechanisms of interaction with plants, we only focused on BGC7 and its product, medpeptin.

3.3. *BGC7 is required for* P. mediterranea *to modulate plant immunity*

We investigated whether the BGC7 mutant had an impact on electrolyte leakage, because it was unable to cause cell death in *N. benthamiana*. The *fliC* mutant of *P. mediterranea* S58 was generated as a control. As expected, S58ΔBGC7 showed a significantly lower conductivity than S58 and S58Δ*fliC* (Fig. 4(a)). To further investigate the impact of BGC7 loss of function on PTI and plant resistance, we examined ROS burst, callose deposition, and challenge inoculation. First, S58 triggered a strong ROS burst, whereas S58Δ*fliC* completely lost ROS production in *N. benthamiana*. Once we silenced *FLAGELLIN SENSING 2* (*fls2*), the receptor of flagellin in *N. benthamiana*, strain S58 could no longer elicit a ROS burst (Fig. 4(b)). This result indicated that flagellin is the major PTI-ROS inducer in *P. mediterranea*. The BGC7 mutant induced the same ROS peak as strain S58, but its ROS production declined more slowly (Fig. 4(b)); moreover, the ROS production induced by BGC7 mutant on *fls2*-silenced plants was similar to that induced by the BGC7/*fliC* double mutant on wild-type plants and declined more slowly than that induced by strain S58 on *fls2*-silenced plants (Fig. 4(b)). This finding implied that BGC7 may be involved in the suppression of weak ROS production induced by other factors in *P. mediterranea*. Strain S58 elicited callose deposition at 24 hpi (Fig. 4(c)), whereas S58Δ*fliC* and S58ΔBGC7 were deficient in callose deposition under the same conditions (Fig. 4(c)). To test pathogen resistance, we infiltrated *N. benthamiana* with strain S58 and the mutants at 1×10^5 CFUs·mL^{-1} and, 6 h later, with the pathogen *Pseudomonas syringae* pv. *tomato* (*Pst*) DC3000Δ*hopQ1-1* at 3×10^4 CFUs·mL^{-1} (Fig. 4(d)). The *fliC* mutant exhibited the same level of pathogen resistance as strain S58 (Fig. 4(d)). In contrast, S58ΔBGC7 showed significantly reduced resistance to *P. syringae* infection. These results collectively indicate that BGC7 and its products contribute to plant immunity and resistance to pathogen infection.

3.4. *Comparative transcriptome analysis reveals a set of immune signaling candidates*

To characterize the immune profile of *N. benthamiana* triggered by strain S58, we performed a transcriptome analysis of six-week-old *N. benthamiana* leaves treated with suspension and crude extracts of strain S58 and S58ΔBGC7. The first analysis of the DEGs for each treatment showed two distinct groups based on the over-

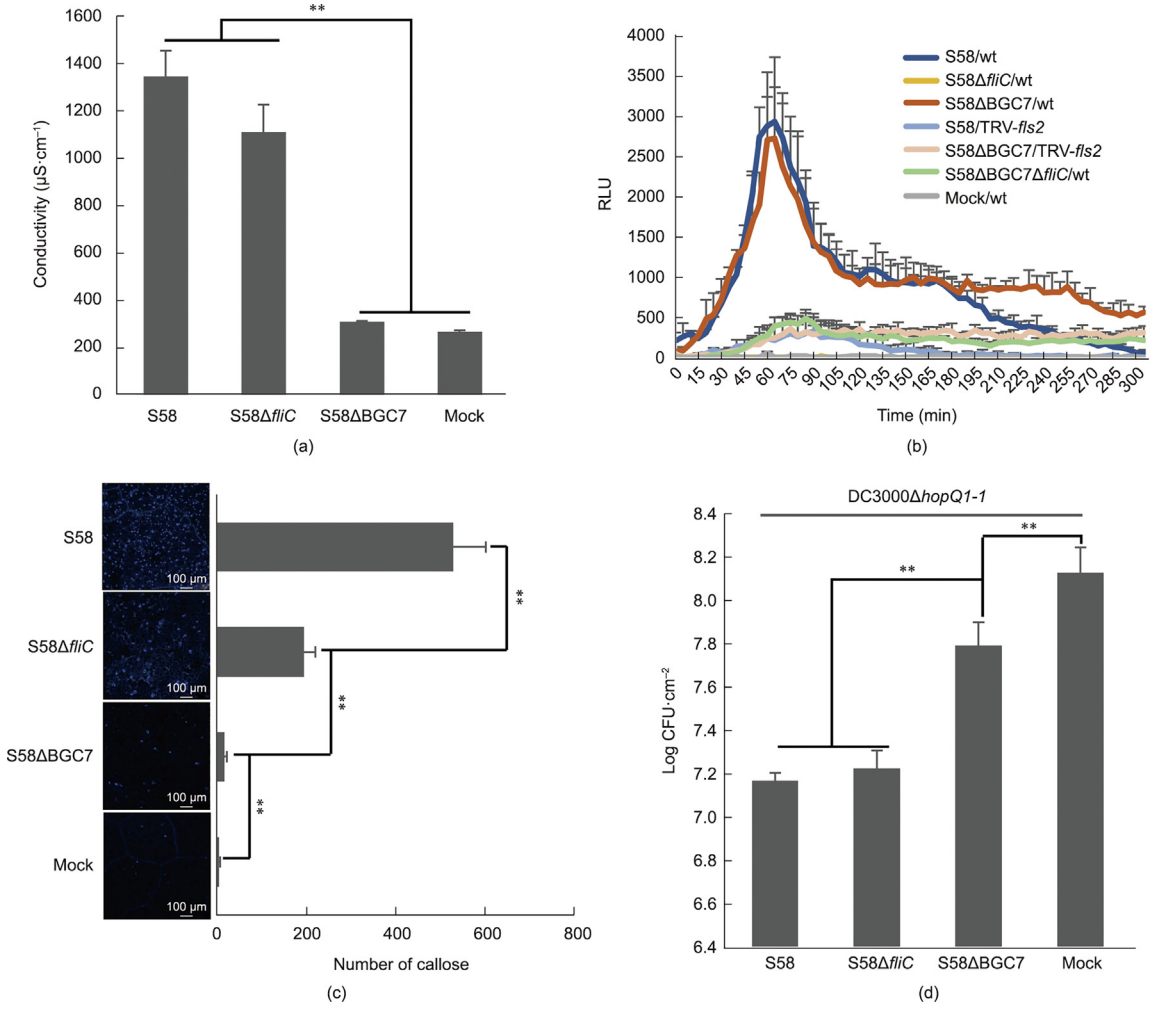

Fig. 4. BGC7 mutation impairs the ability to trigger immune responses. (a) S58ΔBGC7 but not S58Δ*fliC* shows reduced electrolyte leakage in *N. benthamiana* leaves compared with the wild-type strain S58. (b) S58ΔBGC7 has no inhibitory ability against *fliC*-induced early ROS production. wt: wild-type *N. benthamiana*; TRV-*fls2*: *fls2*-silenced *N. benthamiana*. (c) S58ΔBGC7 compromises callose deposition in *N. benthamiana*. The number of callose deposits is shown on the right of each microscopy photograph. (d) S58ΔBGC7 significantly reduces resistance to *Pst* DC3000Δ*hopQ1-1* compared with strain S58. *N. benthamiana* plants were first infiltrated with S58 and derivatives at 1×10^5 CFUs·mL^{-1} and then, 6 h later, infected with 3×10^4 CFUs·mL^{-1} bacterial pathogen suspension. The population of *Pst* DC3000Δ*hopQ1-1* was determined at 4 dpi. Data shown are the means ± SD from three independent plants; ** $P < 0.01$. All experiments were repeated three times, with similar results.

all difference compared with the mock treatment (fold change ≥ 2 and $P < 0.05$). One group had a plenty of DEGs (> 3000; S58 suspension and S58 extract), whereas the other had a much smaller number (< 1500; S58ΔBGC7 suspension and S58ΔBGC7 extract) (Fig. 5(a)). The presence or absence of BGC7 in the treated strains was related to these two extreme responses. Furthermore, the DEGs were grouped into two large clusters by the hierarchical clustering of treatments and DEGs, with cluster B encompassing genes with decreased transcript abundance in the BGC7 mutant treatments (Fig. S2(a) in Appendix A). We discovered a high degree of overlapping genes (1998 genes) whose transcription expression was regulated by both S58 suspension (54.1%) and S58 extract (62.9%), indicating that extracellular secondary metabolites play a major role in plant interactions.

For this study, we focused on the set of genes whose expression was specifically induced by BGC7-derived medpeptin (referred to as *MIG* genes). First, we excluded the 997 genes that were induced by the S58ΔBGC7 suspension and S58ΔBGC7 extract. The remaining 1001 genes were intersected with those whose expression was higher in the S58 suspension than in the S58ΔBGC7 suspension, and higher in the S58 extract than in the S58ΔBGC7 extract. The final 256 genes were identified as *MIG* gene candidates (Fig. 5(b)). We performed GO term analysis using the *N. benthamiana* genome sequence as a reference (Fig. S2(b) and Table S5 in Appendix A). The biological process GO terms of "phospholipid or calcium ion transmembrane transport" and "protein phosphorylation or ubiquitination," which are involved in the mechanical stability of plant cells upon stress stimulation, were mostly enriched. In the "cellular component" category, "integral component of membrane" and "cell periphery" were revealed as the prominent GO terms. Moreover, GO molecular function analysis showed that the majority of the *MIG* gene candidates were enriched in "calcium or ATP binding," "transcription factor (TF)," and "protein kinase (PK)," most of which are involved in immune activation and signaling pathways. To determine the overall transcriptional network response to medpeptin, we performed MapMan analysis[†] to further investigate and visualize the roles of *MIG* genes. The results revealed that the 256 *MIG* genes showed more significant mapping to biotic stress-responsive pathways (Fig. S2(c) in Appendix A), including cell-wall-related processes and hormone signaling, signal transduction, and metabolic pathways. These results indicated that medpeptin functions in plant defense responses by interacting with cell-wall components, regulating hormone production, and altering secondary metabolite biosynthesis.

[†] https://mapman.gabipd.org/.

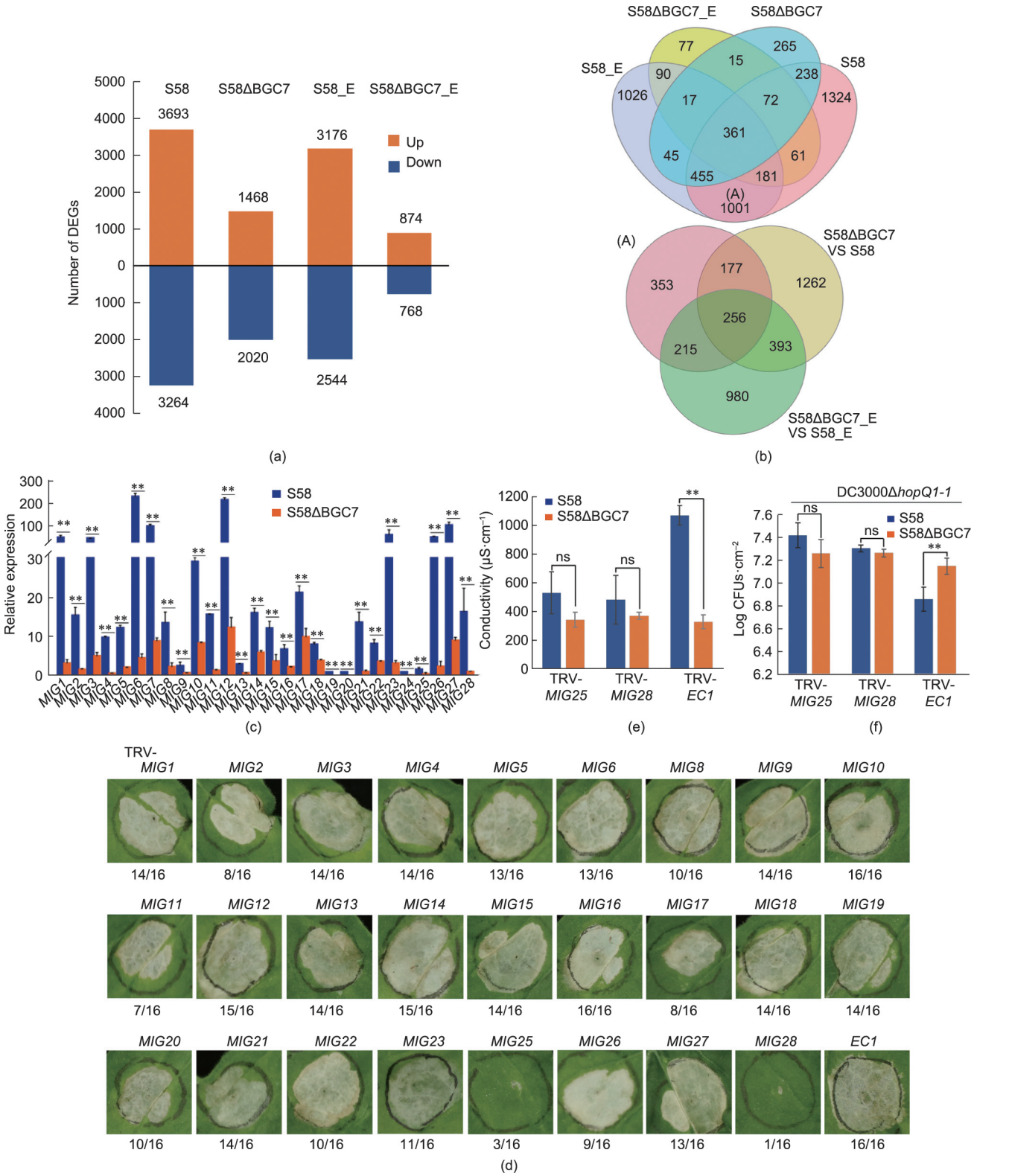

Fig. 5. Screening of medpeptin-induced genes (*MIGs*) in *N. benthamiana*. (a) DEG profiles of *N. benthamiana* treated with S58 suspension, S58ΔBGC7 suspension, extract of S58 (S58_E), and extract of S58ΔBGC7 (S58ΔBGC7_E) compared with 1% methanol (mock). A ≥ 2-fold change and $P < 0.05$ were used as cutoffs. (b) Venn diagram to screen the *MIG* candidates. (c) Relative expression of the 28 *MIG* genes treated by S58 and S58ΔBGC7. *NbEF1α* was used as the reference gene. Relative gene expression was calculated using the $2^{-\Delta\Delta Ct}$ method. (d) Strain S58 triggered cell death in the 28 gene-silenced plants. Strain S58 suspension at 5×10^8 CFUs·mL^{-1} was infiltrated in the relative *N. benthamiana* leaves and photographed at 48 hpi. The fraction under each image indicates the number of times tissue death was observed relative to the number of test inoculations. (e) Silencing of *MIG25* or *MIG28* significantly reduces S58-induced electrolyte leakage. (f) Silencing of *MIG25* or *MIG28* significantly reduces S58-induced resistance against *Pst* DC3000Δ*hopQ1-1* infection. The pathogen population was determined as described in Fig. 4(d). Data shown are the means ± SD from three independent plants; ** $P < 0.01$. All experiments were repeated three times, with similar results. ns: not significant.

Given the significance of PKs and TFs in immune response, we analyzed the families of the two categories of the *MIG* gene candidates. A total of 15 TF families with 30 TF-encoding genes were identified among the 256 *MIG* genes (Fig. S2(d) in Appendix A). The top three families are AF2/ERF, WRKY, and MYB, which include many genes whose roles in the immune response are known: *EFR1*, *WRKY1*, *WRKY18*, and *MYB1* (Table S5) [50–53]. In terms of PKs, we found 21 distributed in 14 families, including the top enriched CAMK_CDPK and RLK_Pelle_LRR (Fig. S2(e) in Appendix A), which drive functions in a variety of biological processes, ranging from cell-wall interactions to disease resistance [54,55]. Taken together, our data revealed previously unknown plant transcriptional reprogramming in *P. mediterranea* medpeptin.

3.5. Silencing of MIG28 and MIG25 compromises cell death immunity

To validate the *MIG* genes, we selected 41 candidates, including transmembrane protein, PK, and TF, based on a thorough bioinformatics analysis (GO and KEGG enrichment analysis) and a literature search for further qRT-PCR testing (Fig. S2(f) and Table S6 in Appendix A). After three rounds of screening, we identified 28 genes whose expression was induced by strain S58 but had significantly lower expression when treated with S58ΔBGC7 (Fig. 5(c)). To identify potential interactions between *MIG* genes, we constructed a model of PPI (i.e., a PPI network) for 28 *Arabidopsis* homologs predicted from *N. benthamiana* (Fig. S3 and Table S7 in Appendix A). The final PPI network was composed of 33 nodes, corresponding to 26 genes involved in 35 interactions, and integrated 78.6% of the *MIG* genes. Three highly connected clusters were generated from the k-means clustering analysis. Remarkably, cluster I contained terms and pathways related to extracellular matrix organization and intracellular signal transduction, especially including the GO terms "response to stimulus," "protein or peptidyl-serine phosphorylation," "calcium-dependent kinase activity," and "cell periphery or plasma membrane." Cluster II was enriched in the nuclear DNA binding associated with the regulation of response to external stimuli and activation of the innate immune response. Cluster III represented terms and pathways related to vesicle docking, exocytosis, cytokinesis, and SNAPE binding. These features suggest that medpeptin may be involved in an integrated PPI network that is composed of immune signaling from the plasma membrane to the nucleus.

To probe the potential impact of *MIG* genes on *P. mediterranea*-induced cell death, we selected 28 genes for analysis using VIGS in *N. benthamiana*. A VIGS construct containing an *E. coli*-derived DNA fragment (*EC1*; see Section 2) was used as a control. We successfully generated VIGS plants for 26 MIG genes, except for *MIG7* and *MIG24*. The VIGS plants showed no discernible changes in growth and morphology but significantly decreased transcript abundance quantified by qRT-PCR (Figs. S4(a) and (b) in Appendix A). Silenced plants were subjected to testing if the candidate gene was involved in cell death triggered by *P. mediterranea* at 5×10^8 CFUs·mL^{-1} for 2 d. Among the 26 candidate genes, we observed a cell-wall LRX gene (*MIG28*, *NbLRX3*, and *Niben101Scf08263g03011.1*) and a receptor-like kinase (RLK) gene (*MIG25*, *NbRLK25*, and *Niben101Scf06437g00005.1*), whose silencing remarkably compromised cell death ($\geq$80%) in any repeat compared with the *EC1* control (Fig. 5(d)). In addition, silencing *MIG2* or *MIG17* moderately impaired cell death ($\geq$1/2), whereas silencing *MIG20*, *MIG22*, or *MIG26* hampered $\geq$1/3 of the cell death induced by *P. mediterranea* S58 (Fig. 5(d)).

Given the notable effects of MIG28 and MIG25, we performed electrolyte leakage and disease assays. *P. mediterranea* S58 induced significantly higher conductivity than S58ΔBGC7 in the *EC1* control plants (Fig. 5(e)). However, the conductivity induced by S58 and S58ΔBGC7 was not significantly different in *MIG28*- or *MIG25*-silenced plants (Fig. 5(e)). Similarly, *P. mediterranea* S58 exhibited significantly stronger resistance to *P. syringae* infection than S58ΔBGC7 in the *EC1* control plants (Fig. 5(f)). Strain S58 lost resistance to pathogen infection once *MIG28* or *MIG25* was silenced, and its growth or disease symptoms were identical to those of S58ΔBGC7 (Fig. 5(f)). These results demonstrated that MIG28 and MIG25 are crucial for the recognition and signal transduction of medpeptin-triggered immunity.

MIG28 and MIG25 are two protein kinases with different domain organizations. The amino acid sequence of the MIG28 protein has 58% identity to *Arabidopsis* LRX3 (AT4G13340.1)—an extracellular protein possessing an N-terminal signal peptide, ten leucine-rich repeats (LRRs), and a C-terminal extensin domain containing hydroxyproline-rich glycoproteins (HRGPs), which are typical structural features of this class. AtLRX3 is a cell-wall-localized protein that is important for the regulation of cell-wall integrity, plant growth, and salt stress tolerance [56]. In comparison, cell-wall leucine-rich repeat extensin protein (NbLRX3) retains the conserved N-terminal signal peptide and LRR domain but has a short and variable extensin domain (Fig. S5(a) in Appendix A). The MIG25 protein is annotated as a serine/threonine tyrosine protein kinase with 52% consensus identity with *Arabidopsis* AT4G10390.1, which is predicted to participate in wound response (GO:0009611). No other domains/motifs or localization signals were found outside of the kinase domain of MIG25 (Fig. S5(b) in Appendix A). A phylogenetic analysis of MIG28 or MIG25 from various plants showed that the two proteins are conserved in dicots, monocots, and other plants, but those from the solanaceous species clustered together (Figs. S6(a) and (b) in Appendix A). Collectively, our findings revealed that bacterial CLPs could modulate plant immunity through cell-wall perception and cytoplastic signaling.

3.6. Medpeptin structure and role in cell death and plant resistance to pathogen infection

Bioinformatics analysis indicated that BGC7 consists of 22 modules, each of which has an A, T, and C domain. The C-terminus of the *mepC* gene encodes two TE domains, implying the termination of medpeptin synthesis (Fig. 6(a)). We previously demonstrated that the relevant *m/z* range of medpeptin is from *m/z* 2050 to *m/z* 2200 by comparing the metabolite profiles of strain S58 and the BGC7 mutant using MALDI-TOF (Fig. 2(b)). We then further examined the extraction of both strains using a more effective liquid chromatography quadrupole time of flight (LC-QTOF; Agilent 1290-6530). The elution profile of strain S58 showed that two major adjacent peaks eluted at 7.17 and 7.25 min were missing in strain S58ΔBGC7 (Fig. 6(b); Fig. S7(a) in Appendix A). The target lipopeptide of the crude extracts after purification by prep-HPLC at the first step were retained in the eluate for 0–15 min; then, the specific fractions were purified again, yielding a monomeric compound with a purity of 93.22% and the highest intensity observed at *m/z* 2107.24 (Figs. S7(b) and (c) in Appendix A). A fragmentation pattern from the MS/MS analysis of the compound combined with data from a direct MALDI-TOF-MS analysis of the partial acid hydrolysates revealed that medpeptin consists of 22 amino acid residues (Dhb-Pro-Ala-Ala-Pro-Val-Val-Dhb-Thr-Val-Ile-Dha-Ala-Ala-Ala-Val-Dhb-Thr-Ala-Dab-Ser-Val) joined to a 3-hydroxy fatty acid tail (Figs. 6(c) and (d); Table S8 in Appendix A). The peptide part of medpeptin contains three nonproteinogenic amino acids—namely, 2,4-diaminobutyric acid (Dab), dehydrobutyrine (Dhb), and dehydroalanine (Dha) (Figs. 6(c)–(e))—which are ubiquitous in some non-ribosomal peptide families, including the tolaasin and syringopeptin groups [3,9]. The primary ion at *m/z* 2107.24

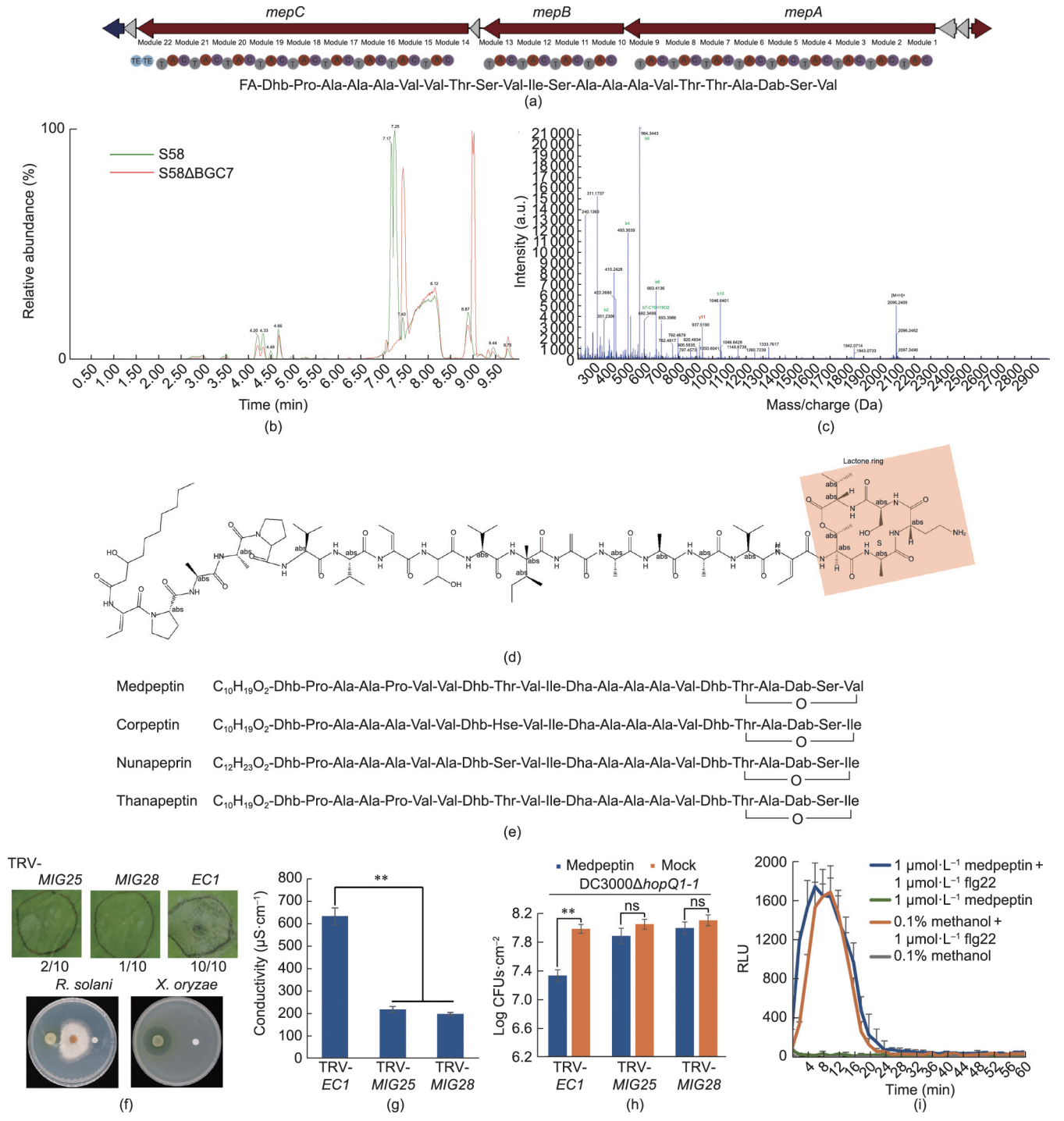

Fig. 6. Structure of medpeptin and its functions in inducing plant immunity. (a) *In silico* prediction of the amino acid composition of medpeptin. The *mepABC* gene cluster is shown, as in Fig. 2(a). A, C, T, and TE domains are shown in different colors. (b) HPLC chromatographic profile of crude extracts from the supernatant of strain S58 and S58ΔBGC7. Two peaks with retention times at 5.17 and 5.25 min are missing in S58ΔBGC7. (c) Ions and amino acid sequence of medpeptin determined using LC-MS/MS. (d) Chemical structure of medpeptin analyzed by genome prediction and LC-MS/MS. (e) Comparison of medpeptin with similar CLPs. The C-terminus of each peptide and a hydroxyl group of a threonine form the macrolactone ring. Hse: homoserine. (f) Medpeptin triggers MIG28- and MIG25-dependent cell death in *N. benthamiana* but does not have antimicrobial activity. Ten microliters of 1 mmol·L^{-1} medpeptin was used to examine cell death in plants and antagonism to plant pathogens. Strain S58 was placed on the left and mutants were placed on the right of each plate. Each treatment had three independent repeats. The fraction under each image indicates the number of times tissue death was observed relative to the number of test inoculations. Antimicrobial activity was measured by the diameter (mm) of the clear zone of growth inhibition. (g) Medpeptin causes electrolyte leakage in *EC1* control plants but not in *MIG25*- or *MIG28*-silenced plants. (h) Medpeptin induces resistance to *Pst* DC3000Δ*hopQ1-1* in *EC1* control plants but not in *MIG25*- or *MIG28*-silenced plants. Medpeptin (100 nmol·L^{-1}) was infiltrated in *N. benthamiana* leaves and, 6 h later, infected with 3×10^4 CFUs·mL^{-1} *Pst* DC3000Δ*hopQ1-1*. The pathogen population was determined as described in Fig. 4(d). (i) Medpeptin neither triggers ROS production nor suppresses ROS burst triggered by flg22. Medpeptin (1 μmol·L^{-1}) was prior infiltrated in the wild-type *N. benthamiana* and, 6 h later, collected for flg22 ROS determination. Data shown are the means ± SD from three independent plants; ** $P < 0.01$. All experiments were repeated three times, with similar results.

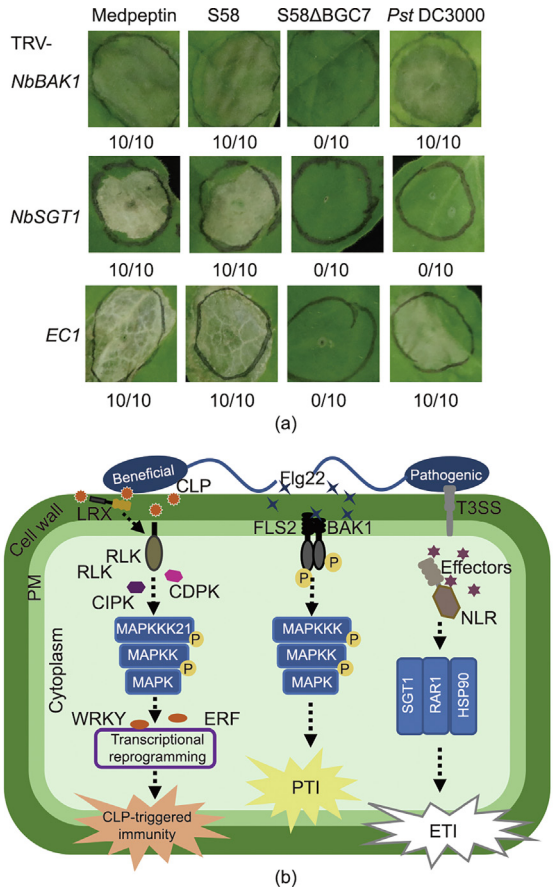

Fig. 7. Schematic diagram of CLP sensing and signaling. (a) *P. mediterranea* S58 and medpeptin triggered cell death independent of BAK1 and SGT1. Medpeptin (1 μmol·L^{-1}), S58, and S58ΔBGC7 (5×10^8 CFUs·mL^{-1}) were infiltrated in *NbBAK1*- and *NbSGT1*-silenced *N. benthamiana*, and Pst DC3000 was used as a nonhost pathogen control. The fraction under each image indicates the number of times tissue death was observed relative to the number of test inoculations. All experiments were repeated three times, with similar results. (b) CLP perception and immune pathway. Beneficial *Pseudomonas* bacteria produce and secrete CLPs, which are sensed by plant cell-wall LRX. Immune signals are transduced to a MAPK cascade through the membrane-bound RLK. The calcium-dependent protein kinase (CDPK) and/or CBL-interacting protein kinase (CIPK) may associate with immune signaling somewhere. Transcriptional factors such as ERF and WRKY bind to and regulate downstream gene expression, stimulating cell death and pathogen resistance. PM: plasma membrane.

$[M + H]^+$ gave a distinct sequence tag for 16 amino acid residues with the sequence Pro-Ala-Ala-Pro-Val-Val-Dhb-Thr-Val-Ile-Dha-Ala-Ala-Ala-Val-Dhb by high-resolution mass spectrometry. Moreover, two larger fragments appeared at *m/z* 254.15 and *m/z* 459.26 in the mass spectrum. The molecular formula of the *m/z* 254.15 fragment correlated with a Dhb residue joined to 3-OH decanoic acid, as with corpeptin and thanapeptin (Fig. 6(e)) [21,49]. The molecular formula for the *m/z* 459.26 fragment possesses a Thr-Ala-Dab-Ser-Val cyclic peptide moiety that is similar to the cyclic tail of corpeptin, nunapeptin, and thanapeptin, except for the last amino acid residue (Fig. 6(e)) [21,48,49].

To confirm that *P. mediterranea* S58-induced plant cell death immunity relies on medpeptin, we examined cell death and disease resistance by using purified medpeptin. Notably, the *EC1* control *N. benthamiana* infiltrated with 1 μmol·L^{-1} medpeptin resulted in complete cell death and electrolyte leakage at 24 hpi, whereas *MIG25*- or *MIG28*-silencing in *N. benthamiana* abolished medpeptin-induced cell death and electrolyte leakage (Figs. 6(f) and (g)). Moreover, prior infiltration with 100 nmol·L^{-1} medpeptin for 6 h significantly reduced pathogen growth compared with the mock control. In contrast, medpeptin failed to control *P. syringae* infection in TRV-MIG25 and TRV-MIG28 plants (Fig. 6(h)). We further investigated the antimicrobial activity, ROS elicitation, callose deposition, expression of PTI- and cell death-related genes, and suppressing activity of medpeptin, and the results demonstrated that medpeptin is unable to antagonize plant pathogens and cannot trigger ROS burst and suppress flg22-triggered ROS production (Figs. 6(f) and (i); Fig. S8(a) in Appendix A). We also noticed that medpeptin can elicit callose deposition and the expression of PTI- and cell death-related genes (Figs. S8(b) and (c) in Appendix A), which is consistent with the findings in S58ΔBGC7 (Figs. 2(a), Fig. 4(b), and 4(c)). These results revealed that medpeptin is the primary cell death inducer produced by *P. mediterranea* S58. It is well known that BAK1 and SGT1 are crucial for PTI and effector-triggered immunity (ETI) (e.g., *Pst* DC3000 HopQ1-1-triggered cell death, Fig. 7(a); Fig. S9 in Appendix A). We investigated whether these two proteins were involved in medpeptin-triggered cell death. We then used VIGS to knock down the expression of *BAK1* and *SGT1* in *N. benthamiana*. However, medpeptin and *P. mediterranea* S58 retained cell death in TRV-*BAK1* and TRV-*SGT1* plants (Fig. 7(a); Fig. S9). Our findings imply that medpeptin-induced cell-surface immunity is distinct from the known PTI and ETI signaling pathways.

4. Discussion

Pseudomonas species—more specifically, the *P. fluorescens* complex—show remarkable metabolic versatility, allowing them to thrive in a variety of ecological niches. Ps-CLPs have been designated as molecular "Swiss Army knives" due to their large structural diversity and broad-spectrum antimicrobial and ecological functions [5]. However, the current understanding of CLP structure–function interactions—particularly CLP perception by plant cells—is still unclear. Here, we discovered that the NRPS gene cluster (BGC7) and its product, medpeptin, are pivotal for *P. mediterranea* S58-induced plant cell death immunity. Further investigation of the transcriptomic network revealed that medpeptin perception requires a set of immune signaling proteins that are distinct from the well-known two-tier immune system. To the best of our knowledge, this is the first report of a Ps-CLP activating cell-surface immunity via cell-wall perception and cytoplastic signaling. This study broadens the array of *Pseudomonas* metabolites used as biological control agents and highlights a new immune network and mechanism involved in CLP-induced plant resistance.

Soil-borne and plant-associated *Pseudomonas* are a large group of CLP-producing bacteria. All known Ps-CLPs can be classified into 14 distinct groups, with multiple homologous members based on the composition and length of the fatty acid tail and the oligopeptide structure [5]. Medpeptin, which was discovered in this study, comprises 22 amino acids in a peptide chain coupled with 3-hydroxy decanoic acid (3-HDA), making it structurally similar to corpeptin, thanapeptin, and braspeptin [21,49,57]. However, medpeptin is unable to inhibit six representative plant pathogens; thus, its activity differs from that of other members of the same group of CLPs, such as nunamycin and nunapeptin from *P. fluorscens* In5. Whether the amino acid variation between medpeptin and these CLPs affects the antimicrobial activity remains to be elucidated. Furthermore, we found a minor peak with a mass of *m/z* 2109 very close to that of medpeptin, however, the effect of the product remains to be elucidated. It has been reported that a single biosynthetic NRPS cluster may produce more than one of the CLPs known as "minor CLPs," which differ in terms of the identity of the amino acids they contain, due to the flexibility of some adenylation domains involved in amino acid recognition [5]. *P. protegens* strains produce orfamide A and orfamide B, which differ by only one amino acid but are equally active against *R. solani* and cause zoospore lysis in *Phytophthora* [19,20]. *Pseudomonas* sp. SH-C52 pro-

duces seven structural variants of thanapeptin, which show varied degrees of activity against *P. infestans* [49]. Although we did not determine the minor peak in *P. mediterranea* S58, studies integrating the utilization of CLP extracts and biosynthesis mutants have revealed that the BGC7 cluster and its product(s) are not responsible for microbial antagonism, ruling out the possibility that the minor CLP is capable of antimicrobial activity. In this study, we demonstrated that the *Pseudomonas* QS system strictly controlled not only the production of medpeptin but also the antagonism derived from unknown metabolites against phytopathogenic fungi and gram-negative bacteria. Interestingly, the vast majority of Ps-CLPs are inactive against Gram-negative bacteria [5], implying that *P. mediterranea* recruits diverse antimicrobial metabolites to inhibit different pathogen classes. Given that *P. mediterranea* is metabolically versatile, according to our *in silico* genome analysis, intensive research to prescribe a metabolic "package" for specific pathogens will significantly advance precision plant protection.

CLPs are capable of inducing plant immune resistance to prime plant protection against diseases, in addition to acting directly on the pathogen via antimicrobial properties [3,58]. It is intriguing that medpeptin only induces plant resistance and does not have antimicrobial activity, making it completely distinct from general Ps-CLPs. Given this unique property, medpeptin has the potential to be developed into a new plant health promoter that only activates plant immune systems and does not perturb microbial commensalism. In this study, using a rigorous combination of chemical extractions and bacterial mutants, we demonstrated that medpeptin from *P. mediterranea* is sufficient to induce immune responses via an NbLRX3- and a receptor-like protein kinase (NbRLK25)-mediated pathway in *N. benthamiana*. LRXs are chimeric proteins that insolubilize in the cell wall and create platforms for protein-protein interaction [59]. Interestingly, LRX3/LRX4/LRX5 proteins have been shown to bind to the plant endogenous peptide rapid alkalanization factors (RALFs) with high affinity [56,60,61]. Due to the lack of an intracellular domain, LRX proteins recruit *Catharanthus roseus* receptor-like protein kinase 1-like (CrRLK1L) FERONIA (FER) to transduce cell-wall signals into the cell interior, regulating cell-wall integrity, root hair morphogenesis, and salt stress tolerance [56,60–62]. Furthermore, a recent study showed that LRXs and FER regulate BAK1 nanoscale organization, and that the *lrx3/4/5* triple mutant is impaired in PTI ROS production, indicating that FER and LRXs have functional dichotomy in regulating development and immunity [26]. Although there is no evidence so far that FER is associated with medpeptin-triggered immunity, we showed that BAK1 (Fig. 7(a)), FLS2, MKK2, SIPK, and WIPK are not required in this process (data not shown), ruling out the possibility that medpeptin activates plant immunity via the LRXs–FER–BAK1 pathway. We also examined whether medpeptin signaling is associated with typical ETI regulators. However, silencing SGT1 (Fig. 7(a)), RAR1, HSP90, EDS1, and NDR1 (data not shown) did not alter medpeptin-triggered cell death in *N. benthamiana*.

Our observations support a model of Ps-CLP perception and downstream signaling in plants (Fig. 7(b)). In contrast to PRR-mediated PTI and NLR-mediated ETI, medpeptin-like CLPs produced by beneficial *Pseudomonas* are sensed directly or indirectly by cell-wall LRX. Immune signals are transduced through plasma membrane-bound RLK to the cytoplasm and activate downstream signaling such as the MAPK cascade, where the CDPK and/or CBL-interacting protein kinase (CIPK) may be involved in plant defense signaling. Thereafter, transcriptional factors, such as ERF and WRKY, bind to and regulate downstream gene expression, stimulating cell death and resistance to pathogens. Given the structural similarity of Ps-CLPs in *Pseudomonas*, enhanced mechanistic insights into CLP signaling would open up new perspectives for the development of plant resistance against pathogen infection.

5. Conclusions

In this study, we identified medpeptin, a novel cyclic lipopeptide from *P. mediterranea*, and characterized its structure and regulatory mechanisms. Further investigation of the transcriptomic network of *N. benthamiana* revealed that medpeptin perception implies a set of immune signaling proteins distinct from the well-known two-tier immune system. VIGS revealed that medpeptin-induced cell death and pathogen resistance are dependent on a NbLRX3 and a NbRLK25. Our findings point to a non-canonical mechanism of CLP sensing and suggest avenues for the development of plant disease resistance. To the best of our knowledge, this is the first report of a Ps-CLP modulating plant immunity via cell-wall perception and cytoplastic signaling.

Acknowledgments

We thank Dr. Yuquan Xu (Biotechnology Research Institute, CAAS) for technical assistance with MALDI-TOF and LC-MS/MS. This work is funded by the National Key R&D Program of China (2022YFD1901300), the National Natural Science Foundation of China (31901932), the Agricultural Science and Technology Innovation Program of Chinese Academy of Agricultural Sciences (CAAS-ZDRW202308 and Y2022PT12), the Beijing Innovation Consortium of Agriculture Research System (BAIC04-2022), and the Science and Technology Programs of the Zunyi Tobacco (2021XM03).

Compliance with ethics guidelines

Yi-Lin Gu, Jun-Zhou Li, Yan Li, Shen Cong, Jing Wang, Yi-Nan Ma, and Hai-Lei Wei declare that they have no conflict of interest or financial conflicts to disclose.

Appendix A. Supplementary data

Supplementary data to this article can be found online at https://doi.org/10.1016/j.eng.2023.05.016.

References

[1] Haas D, Défago G. Biological control of soil-borne pathogens by fluorescent pseudomonads. Nat Rev Microbiol 2005;3(4):307–19.
[2] Girard L, Geudens N, Pauwels B, Höfte M, Martins JC, De Mot R. Transporter gene-mediated typing for detection and genome mining of lipopeptide-producing *Pseudomonas*. Appl Environ Microbiol 2022;88(2):e0186921.
[3] Raaijmakers JM, de Bruijn I, de Kock MJ. Cyclic lipopeptide production by plant-associated *Pseudomonas* spp.: diversity, activity, biosynthesis, and regulation. Mol Plant Microbe Interact 2006;19(7):699–710.
[4] Oni FE, Esmaeel Q, Onyeka JT, Adeleke R, Jacquard C, Clement C, et al. *Pseudomonas* lipopeptide-mediated biocontrol: chemotaxonomy and biological activity. Molecules 2022;27(2):372.
[5] Geudens N, Martins JC. Cyclic lipodepsipeptides from *Pseudomonas* spp.—biological swiss-army knives. Front Microbiol 2018;1867:9.
[6] Finking R, Marahiel MA. Biosynthesis of nonribosomal peptides. Annu Rev Microbiol 2004;58:453–88.
[7] Götze S, Stallforth P. Structure, properties, and biological functions of nonribosomal lipopeptides from pseudomonads. Nat Prod Rep 2020;37(1):29–54.
[8] De Bruijn I, Raaijmakers JM. Diversity and functional analysis of LuxR-type transcriptional regulators of cyclic lipopeptide biosynthesis in *Pseudomonas fluorescens*. Appl Environ Microbiol 2009;75(14):4753–61.
[9] Gross H, Loper JE. Genomics of secondary metabolite production by *Pseudomonas* spp. Nat Prod Rep 2009;26(11):1408–46.
[10] Licciardello G, Bertani I, Steindler L, Bella P, Venturi V, Catara V. *Pseudomonas corrugata* contains a conserved *N*-acyl homoserine lactone quorum sensing system; its role in tomato pathogenicity and tobacco hypersensitivity response. FEMS Microbiol Ecol 2007;61(2):222–34.
[11] Licciardello G, Strano CP, Bertani I, Bella P, Fiore A, Fogliano V, et al. *N*-acyl-homoserine-lactone quorum sensing in tomato phytopathogenic *Pseudomonas* spp. is involved in the regulation of lipodepsipeptide production. J Biotechnol 2012;159(4):274–82.

[12] Licciardello G, Caruso A, Bella P, Gheleri R, Strano CP, Anzalone A, et al. The LuxR regulators PcoR and RfiA co-regulate antimicrobial peptide and alginate production in *Pseudomonas corrugata*. Front Microbiol 2018;9(4):521.
[13] Hennessy RC, Phippen CBW, Nielsen KF, Olsson S, Stougaard P. Biosynthesis of the antimicrobial cyclic lipopeptides nunamycin and nunapeptin by *Pseudomonas fluorescens* strain In5 is regulated by the LuxR-type transcriptional regulator NunF. MicrobiologyOpen 2017;6(6):e00516.
[14] Schellenberger R, Touchard M, Clément C, Baillieul F, Cordelier S, Crouzet J, et al. Apoplastic invasion patterns triggering plant immunity: plasma membrane sensing at the frontline. Mol Plant Pathol 2019;20(11):1602–16.
[15] Ngou BPM, Ding P, Jones JDG. Thirty years of resistance: zig–zag through the plant immune system. Plant Cell 2022;34(5):1447–78.
[16] Tran H, Ficke A, Asiimwe T, Höfte M, Raaijmakers JM. Role of the cyclic lipopeptide massetolide A in biological control of *Phytophthora infestans* and in colonization of tomato plants by *Pseudomonas fluorescens*. New Phytol 2007;175(4):731–42.
[17] Jang JY, Yang SY, Kim YC, Lee CW, Park MS, Kim JC, et al. Identification of orfamide A as an insecticidal metabolite produced by *Pseudomonas protegens* F6. J Agric Food Chem 2013;61(28):6786–91.
[18] Olorunleke FE, Hua GKH, Kieu NP, Ma Z, Höfte M. Interplay between orfamides, sessilins and phenazines in the control of Rhizoctonia diseases by *Pseudomonas* sp. CMR12a. Environ Microbiol Rep 2015;7(5):774–81.
[19] Ma Z, Hua GKH, Ongena M, Höfte M. Role of phenazines and cyclic lipopeptides produced by *Pseudomonas* sp. CMR12a in induced systemic resistance on rice and bean. Environ Microbiol Rep 2016;8(5):896–904.
[20] Ma Z, Ongena M, Höfte M. The cyclic lipopeptide orfamide induces systemic resistance in rice to *Cochliobolus miyabeanus* but not to *Magnaporthe oryzae*. Plant Cell Rep 2017;36(11):1731–46.
[21] Emanuele MC, Scaloni A, Lavermicocca P, Jacobellis NS, Camoni L, Di Giorgio D, et al. Corpeptins, new bioactive lipodepsipeptides from cultures of *Pseudomonas corrugata*. FEBS Lett 1998;433(3):317–20.
[22] Strano CP, Bella P, Licciardello G, Fiore A, Lo Piero AR, Fogliano V, et al. *Pseudomonas corrugata* crpCDE is part of the cyclic lipopeptide corpeptin biosynthetic gene cluster and is involved in bacterial virulence in tomato and in hypersensitive response in *Nicotiana benthamiana*. Mol Plant Pathol 2015;16(5):495–506.
[23] Ranf S, Gisch N, Schäffer M, Illig T, Westphal L, Knirel YA, et al. A lectin S-domain receptor kinase mediates lipopolysaccharide sensing in *Arabidopsis thaliana*. Nat Immunol 2015;16(4):426–33.
[24] Kutschera A, Dawid C, Gisch N, Schmid C, Raasch L, Gerster T, et al. Bacterial medium-chain 3-hydroxy fatty acid metabolites trigger immunity in *Arabidopsis* plants. Science 2019;364(6436):178–81.
[25] Schellenberger R, Crouzet J, Nickzad A, Shu LJ, Kutschera A, Gerster T, et al. Bacterial rhamnolipids and their 3-hydroxyalkanoate precursors activate *Arabidopsis* innate immunity through two independent mechanisms. Proc Natl Acad Sci USA 2021;118(39):e2101366118.
[26] Gronnier J, Franck CM, Stegmann M, DeFalco TA, Abarca A, von Arx M, et al. Regulation of immune receptor kinase plasma membrane nanoscale organization by a plant peptide hormone and its receptors. eLife 2022;11:e74162.
[27] Gu Y, Wang J, Xia Z, Wei H. Characterization of a versatile plant growth-promoting rhizobacterium *Pseudomonas mediterranea* strain S58. Microorganisms 2020;8(3):334.
[28] King EO, Ward MK, Raney DE. Two simple media for the demonstration of pyocyanin and fluorescin. J Lab Clin Med 1954;44(2):301–7.
[29] Herrero M, de Lorenzo V, Timmis KN. Transposon vectors containing non-antibiotic resistance selection markers for cloning and stable chromosomal insertion of foreign genes in gram-negative bacteria. J Bacteriol 1990;172(11):6557–67.
[30] Wei HL, Chakravarthy S, Mathieu J, Helmann TC, Stodghill P, Swingle B, et al. *Pseudomonas syringae* pv. tomato DC3000 type III secretion effector polymutants reveal an interplay between HopAD1 and AvrPtoB. Cell Host Microbe 2015;17(6):752–62.
[31] Li X, Gu G, Chen W, Gao L, Wu X, Zhang L. The outer membrane protein OprF and the sigma factor SigX regulate antibiotic production in *Pseudomonas fluorescens* 2P24. Microbiol Res 2018;206:159–67.
[32] Skinnider MA, Johnston CW, Gunabalasingam M, Merwin NJ, Kieliszek AM, MacLellan RJ, et al. Comprehensive prediction of secondary metabolite structure and biological activity from microbial genome sequences. Nat Commun 2020;11(1):6058.
[33] De la Torre F, Gutiérrez-Beltrán E, Pareja-Jaime Y, Chakravarthy S, Martin GB, del Pozo O. The tomato calcium sensor Cbl10 and its interacting protein kinase Cipk6 define a signaling pathway in plant immunity. Plant Cell 2013;25(7):2748–64.
[34] Zhang M, Chiang YH, Toruño TY, Lee D, Ma M, Liang X, et al. The MAP4 kinase SIK1 ensures robust extracellular ROS burst and antibacterial immunity in plants. Cell Host Microbe 2018;24(3):379–91.e5.
[35] Li B, Ferreira MA, Huang M, Camargos LF, Yu X, Teixeira RM, et al. The receptor-like kinase NIK1 targets FLS2/BAK1 immune complex and inversely modulates antiviral and antibacterial immunity. Nat Commun 2019;10:4996.
[36] Katiyar-Agarwal S, Morgan R, Dahlbeck D, Borsani O, Villegas Jr A, Zhu JK, et al. A pathogen-inducible endogenous siRNA in plant immunity. Proc Natl Acad Sci USA 2006;103(47):18002–7.
[37] Bombarely A, Rosli HG, Vrebalov J, Moffett P, Mueller LA, Martin GB. A draft genome sequence of *Nicotiana benthamiana* to enhance molecular plant-microbe biology research. Mol Plant Microbe Interact 2012;25(12):1523–30.
[38] Love MI, Huber W, Anders S. Moderated estimation of fold change and dispersion for RNA-seq data with DESeq2. Genome Biol 2014;15(12):550.
[39] Heberle H, Meirelles GV, da Silva FR, Telles GP, Minghim R. InteractiVenn: a web-based tool for the analysis of sets through Venn diagrams. BMC Bioinformatics 2015;16(1):169.
[40] Thimm O, Bläsing O, Gibon Y, Nagel A, Meyer S, Krüger P, et al. MAPMAN: a user-driven tool to display genomics data sets onto diagrams of metabolic pathways and other biological processes. Plant J 2004;37(6):914–39.
[41] Szklarczyk D, Gable AL, Lyon D, Junge A, Wyder S, Huerta-Cepas J, et al. STRING v11: protein–protein association networks with increased coverage, supporting functional discovery in genome-wide experimental datasets. Nucleic Acids Res 2019;47(D1):D607–13.
[42] Fernandez-Pozo N, Rosli HG, Martin GB, Mueller LA. The SGN VIGS tool: user-friendly software to design virus-induced gene silencing (VIGS) constructs for functional genomics. Mol Plant 2015;8(3):486–8.
[43] Liu Y, Schiff M, Dinesh-Kumar SP. Virus-induced gene silencing in tomato. Plant J 2002;31(6):777–86.
[44] Senthil-Kumar M, Mysore KS. Tobacco rattle virus-based virus-induced gene silencing in *Nicotiana benthamiana*. Nat Protoc 2014;9(7):1549–62.
[45] Oh CS, Martin GB. Tomato 14-3-3 protein TFT7 interacts with a MAP kinase kinase to regulate immunity-associated programmed cell death mediated by diverse disease resistance proteins. J Biol Chem 2011;286(16):14129–36.
[46] Velásquez AC, Chakravarthy S, Martin GB. Virus-induced gene silencing (VIGS) in *Nicotiana benthamiana* and tomato. J Vis Exp 2009;28:e1292.
[47] Sikorski J, Jahr H, Wackernagel W. The structure of a local population of phytopathogenic *Pseudomonas brassicacearum* from agricultural soil indicates development under purifying selection pressure. Environ Microbiol 2001;3(3):176–86.
[48] Michelsen CF, Watrous J, Glaring MA, Kersten R, Koyama N, Dorrestein PC, et al. Nonribosomal peptides, key biocontrol components for *Pseudomonas fluorescens* In5, isolated from a Greenlandic suppressive soil. MBio 2015;6(2):e00079–e115.
[49] Van Der Voort M, Meijer HJG, Schmidt Y, Watrous J, Dekkers E, Mendes R, et al. Genome mining and metabolic profiling of the rhizosphere bacterium *Pseudomonas* sp. SH-C52 for antimicrobial compounds. Front Microbiol 2015;6:693.
[50] Yang Y, Klessig DF. Isolation and characterization of a tobacco mosaic virus-inducible *myb* oncogene homolog from tobacco. Proc Natl Acad Sci USA 1996;93(25):14972–7.
[51] Lorenzo O, Piqueras R, Sánchez-Serrano JJ, Solano R. ETHYLENE RESPONSE FACTOR1 integrates signals from ethylene and jasmonate pathways in plant defense. Plant Cell 2003;15(1):165–78.
[52] Wang D, Amornsiripanitch N, Dong X. A genomic approach to identify regulatory nodes in the transcriptional network of systemic acquired resistance in plants. PLoS Pathog 2006;2(11):e123.
[53] Shinde BA, Dholakia BB, Hussain K, Aharoni A, Giri AP, Kamble AC. *WRKY1* acts as a key component improving resistance against *Alternaria solani* in wild tomato, *Solanum arcanum Peralta*. Plant Biotechnol J 2018;16(8):1502–13.
[54] Gish LA, Clark SE. The RLK/Pelle family of kinases. Plant J 2011;66(1):117–27.
[55] Wang JP, Xu YP, Munyampundu JP, Liu TY, Cai XZ. Calcium-dependent protein kinase (CDPK) and CDPK-related kinase (CRK) gene families in tomato: genome-wide identification and functional analyses in disease resistance. Mol Genet Genomics 2016;291(2):661–76.
[56] Herger A, Dünser K, Kleine-Vehn J, Ringli C. Leucine-rich repeat extensin proteins and their role in cell wall sensing. Curr Biol 2019;29(17):R851–8.
[57] Zhao H, Liu Y, Zhang L. *In silico* and genetic analyses of cyclic lipopeptide synthetic gene clusters in *Pseudomonas* sp. 11K1. Front Microbiol 2019;10:544.
[58] Pršić J, Ongena M. Elicitors of plant immunity triggered by beneficial bacteria. Front Plant Sci 2020;11:594530.
[59] Mecchia MA, Santos-Fernandez G, Duss NN, Somoza SC, Boisson-Dernier A, Gagliardini V, et al. RALF4/19 peptides interact with LRX proteins to control pollen tube growth in *Arabidopsis*. Science 2017;358(6370):1600–3.
[60] Zhao C, Zayed O, Yu Z, Jiang W, Zhu P, Hsu CC, et al. Leucine-rich repeat extensin proteins regulate plant salt tolerance in *Arabidopsis*. Proc Natl Acad Sci USA 2018;115(51):13123–8.
[61] Dünser K, Gupta S, Herger A, Feraru MI, Ringli C, Kleine-Vehn J. Extracellular matrix sensing by FERONIA and leucine-rich repeat extensins controls vacuolar expansion during cellular elongation in *Arabidopsis thaliana*. EMBO J 2019;38(7):e100353.
[62] Zhao C, Jiang W, Zayed O, Liu X, Tang K, Nie W, et al. The LRXs-RALFs-FER module controls plant growth and salt stress responses by modulating multiple plant hormones. Natl Sci Rev 2020;8(1):nwaa149.